Physical Communication 17 (2015) 172–184

Contents lists available at ScienceDirect

Physical Communication

journal homepage: www.elsevier.com/locate/phycom

Full length article

Design and implementation of spectrum sensing for cognitive radios with a frequency-hopping primary system☆

Sanjeev Gurugopinath *, Raghavendra Akula, Chandra R. Murthy, Prasanna R., Bharadwaj Amrutur

Department of ECE, Indian Institute of Science, Bangalore, 560 012, India

ARTICLE INFO

Article history:
Received 28 August 2014
Received in revised form 3 September 2015
Accepted 4 September 2015
Available online 30 September 2015

Keywords:
Spectrum sensing
Frequency-hopping primary
FAR algorithm
Software defined radio

ABSTRACT

In this work, spectrum sensing for cognitive radios is considered in the presence of multiple Primary Users (PU) using frequency-hopping communication over a set of frequency bands. The detection performance of the Fast Fourier Transform (FFT) Average Ratio (FAR) algorithm is obtained in closed-form, for a given FFT size and number of PUs. The effective throughput of the Secondary Users (SU) is formulated as an optimization problem with a constraint on the maximum allowable interference on the primary network. Given the hopping period of the PUs, the sensing duration that maximizes the SU throughput is derived. The results are validated using Monte Carlo simulations. Further, an implementation of the FAR algorithm on the Lyrtech (now, Nutaq) small form factor software defined radio development platform is presented, and the performance recorded through the hardware is observed to corroborate well with that obtained through simulations, allowing for implementation losses.

1. Introduction

A *Cognitive Radio* (CR) [2] operates by *sensing* the spectrum for *Primary User* (PU) activity, and transmitting only in frequency bands where the PU signal is observed to be absent. The detection of PU activity is accomplished via Spectrum Sensing (SS), which is the binary hypothesis testing problem of detecting the presence or absence of a PU in a frequency-band of interest. SS has received significant research attention over the past decade (see [3–5] for recent tutorial surveys on the topic). Some of the popular algorithms include Energy Detection (ED), matched filter detection, cyclostationary detection, etc. Energy based detection, which uses the received signal energy to construct the decision statistic, is popular because it is simple, easy to implement, and does not assume any information about the structure of the PU signal [6]. However, ED requires accurate knowledge of the noise variance, and its performance degrades due to noise variance uncertainty [7,8].

In order to maximize the throughput of the CR while simultaneously offering adequate protection to the primary, it is important to tune the various sensing and transmission related parameters, such as the sensing duration, threshold, transmit power, etc., considering the primary signal characteristics. The problem of SS is particularly challenging when the primary users employ Frequency Hopping (FH) signaling, since the CR needs to detect and exploit the available frequency bins within the short hop duration of the primary.

☆ This work has appeared in part in [1].

* Corresponding author.
E-mail addresses: sanjeev.g@ece.iisc.ernet.in (S. Gurugopinath), ragi.surya@gmail.com (R. Akula), cmurthy@ece.iisc.ernet.in (C.R. Murthy), prasanna.ceg@gmail.com (P. R.), amrutur@ece.iisc.ernet.in (B. Amrutur).

http://dx.doi.org/10.1016/j.phycom.2015.09.001
1874-4907/

The focus of this paper is on the detection of FH primary signals. FH signals are typically used in many secure/military and commercial applications [9], navigation-related applications [10], and in the standards such as IEEE 802.15.1/ Bluetooth [11,12]. SS of FH primary signals is challenging due to the frequently changing nature of the primary frequency band, and has received relatively less attention in the CR literature. Some work on the detection of frequency-hopped signals, albeit in a non-CR context, include [13–15]. In these studies, the received signal is passed through a bank of Band Pass Filters (BPFs), and a decision on the signal presence in each frequency bin is made from the energy computed in each BPF, in time domain. In [16], a Fast Fourier Transform (FFT)-based CFAR detection scheme, based on the Cell Averaging Constant False-Alarm Rate (CA-CFAR) [17,18], which we call as the FFT Averaging Ratio (FAR) algorithm in this paper, was proposed for wideband spectrum sensing, which is applicable to the detection of the presence or absence of FH primary signals. Although known to be less robust as compared to several other alternative detection techniques, we choose to work with the FAR algorithm because of its simplicity and analytical tractability. In terms of implementation on a hardware platform, spectrum sensing has been recently demonstrated in a non-FH primary environment using off-the-shelf software defined radio platforms [19–23].

To the best of our knowledge, however, past work on detecting FH signals has focused primarily on detecting the presence or absence of an FH primary signal itself (e.g., [16], [12]), not on detecting and harvesting unoccupied bands for CR communication within each hop duration. That is, if the primary is declared present, then none of the frequency bins used by the primary are allowed to be used by the CR. If the primary is declared absent, the CR communicates using all of the frequency bins over which the primary previously employed FH communication. In the FH-primary case, in each hop duration, the active primaries occupy only a small subset of the available frequency bins. Most of the frequency bins are left unoccupied, and can be opportunistically accessed by the CR users, provided they are able to perform fast sensing and find an unoccupied frequency bin (or a set of unoccupied frequency bins) within each hop duration. In this work, we investigate the possibility of the CR users opportunistically accessing the bins within the hop-space of the primary that are unoccupied in each hop duration, as against waiting for all the primary users to be silent before reusing the spectrum. The goal here is to find unoccupied frequency bins within each hop duration for the CR to communicate in short bursts, thereby communicating in the same wideband frequency range as the primary, but without causing interference. To this end, in this paper, we consider energy-based detection of unoccupied bands in the presence of FH primary signals, and evaluate its efficacy through rigorous theoretical analysis, Monte Carlo simulations, and implementation on a hardware platform. Some studies in the literature do assume a scenario where the CR users employ a time-slotted communication scheme, with the initial part being used for sensing and the later part for communication [24,25]. However, to the best of our knowledge, ours is the first work that considers a cross-layer approach for finding and reusing the available frequency bins *within* the hop duration of an FH primary.

Our contributions are as follows:

- We extend the FAR algorithm [16] for detecting unoccupied frequency bins within the hop duration in a multiuser FH-PU scenario, and derive closed-form expressions for the probabilities of false alarm and detection, as a function of the detection threshold, number of averaging frames, and the SNRs of the primary signal in the occupied bands (Section 3.1). We consider the FAR algorithm for detection because of its computational simplicity and ease of implementation in a software defined radio environment.
- We define a utility metric to quantify the throughput of the CR, and obtain the CR sensing duration that maximizes the throughput while satisfying a constraint on the maximum allowable interference to the PUs (Section 3.2).
- We implement the FAR Algorithm on a Lyrtech (now. Nutaq) Small Form Factor Software Defined Radio Development Platform (Lyrtech SFF SDR DP), and validate the implementation by comparing its performance with that obtained from the analysis and simulations (Sections 4 and 5).

Allowing for implementation losses of about 1 dB, the results obtained from the hardware corroborate well with those obtained through theory as well as Monte Carlo simulations. We conclude, therefore, that the FAR algorithm is an easy-to-implement and effective solution to the SS problem with an FH-PU network.

The rest of the paper is organized as follows. The system model and the FAR algorithm are given in Section 2. The associated probabilities of false-alarm and detection of the FAR algorithm as applied to SS with FH primary signals are derived in Section 3.1, and the optimum sensing duration that maximizes the CR throughput is derived in Section 3.2. The implementation of the FAR algorithm on the Lyrtech SFF SDR DP is discussed in Section 4. Finally, Section 5 discusses Monte-Carlo simulations and experimental results, and Section 6 concludes the paper.

2. System model and FAR algorithm

2.1. System model

In an FH network, each PU occupies a frequency bin for a period of time, known as the hopping period, or the hop duration (N_h samples). In successive hop periods, the PUs synchronously switch to new frequency bins chosen according a pseudo-random sequence. The hop sequence followed by the primary users is not available at the CR nodes. Hence, in each hop duration, the task of the CR is to identify unoccupied frequency bins as quickly as possible and transmit its data, before sensing again during the next hop period of the primary network.

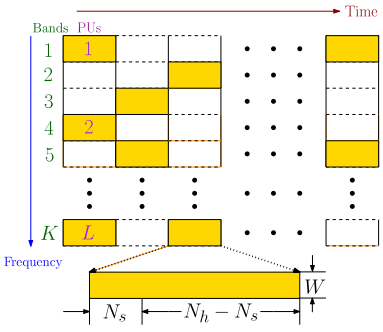

Fig. 1. Typical frequency-band occupancies in a multiple FH-PU network.

Suppose the CR wishes to find a spectrum hole of bandwidth W Hz within a wider band of interest of bandwidth B Hz. Let $B = KW$ i.e., the bandwidth B consists of K contiguous, non-overlapping bins (Bartlett spectrum estimation technique). In our model, W is fixed. It is equal to the bandwidth of a single frequency bin of the FH primary system; and we assume that the CR operates in chunks of bandwidth W. We assume that, at any given hop duration, each active primary user occupies one of the K bins, as shown in Fig. 1. The shaded bins in Fig. 1 represent the bins occupied by the PUs at some given hop interval; there are L active PUs in the figure. The pseudo-random primary signal hopping pattern is unknown to the CR users, and can be well modeled as an i.i.d. random sequence, independent across users, and uniformly distributed over the K bins [15,26]. In general, this hopping sequence can be random, or predefined and deterministic. Since the hopping sequence is unknown at the CR users, they need to sense the spectrum to find empty frequency bins prior to communicating. If the primary hopping sequence is known at the CR users, the problem becomes almost trivial: the CR users can pick any or all of the frequency bins that are unoccupied in each hop duration, and use them for the secondary communications. The CR down-converts the received signal, band-limits it to B Hz, and samples it at a rate of $f_s \geq 2B$ samples/s. In this paper, for simplicity, we assume that the number of active PUs, denoted by L, is known. In practice, since the number of active PUs typically varies very slowly compared to the bin occupancy patterns, it can be estimated and tracked based on the sensing outcomes [27]. Let $\mathbf{u} \in \{0, 1\}^K$ represent the primary occupancy pattern, where $\mathbf{u}(k)$ takes the value 0 or 1, depending on whether the kth frequency band is free or occupied, respectively.

The CR collects $N_s = NM$ data samples, groups them into M frames of N samples each, and applies an N-point FFT on each frame (possibly, with windowing, to control the side-lobes) [28,29]. Thus, the sensing duration is N_s/f_s. Also, N is chosen to be a positive integer multiple of K, and an integer power of 2. In each frame, multiple FFT bins are grouped to represent the samples from each of the K PU bands. This is done to reduce the spectral leakage due to the FFT. For every N_s, there are many combinations of M and N possible. In our analysis, we fix N and vary M, since, in practical implementations, N is fixed based on the hardware capability. The received baseband samples in mth frame are represented as [1]

$$\bar{y}_m = \bar{x}_m + \bar{z}_m, \quad m = 0, 1, \ldots, M-1,$$

where $\bar{y}_m \triangleq \left[y_m[0], y_m[1], \ldots, y_m[N-1]\right]^T$, $\bar{x}_m \triangleq \left[x_m[0], x_m[1], \ldots, x_m[N-1]\right]^T$ and $\bar{z}_m \triangleq \left[z_m[0], z_m[1], \ldots, z_m[N-1]\right]^T$ represent the received samples, the received PU signal component and the thermal noise component at the receiver, respectively. We assume that $z_m[n] \sim \mathcal{CN}(0, \sigma^2)$, and i.i.d. across all m, n, where $\mathcal{CN}(\mu, \nu)$ represents a circularly symmetric complex Gaussian distribution with mean μ and variance ν.

Let Q represent the $N \times N$ FFT matrix, with (p, q)th entry equal to $\frac{1}{\sqrt{N}} \exp\{-j\frac{2\pi pq}{N}\}$, $0 \leq p, q \leq N-1$. Let $\bar{Y}_m \triangleq Q\bar{y}_m$, $\bar{X}_m \triangleq Q\bar{x}_m$ and $\bar{Z}_m \triangleq Q\bar{z}_m$. When the kth band is vacant, the samples in the (N/K) frequency bins corresponding to the kth band are modeled as [29]

$$\bar{Y}_m(\ell) = \bar{Z}_m(\ell), \quad \ell = \frac{kN}{K}, \frac{kN}{K} + 1, \ldots, \frac{(k+1)N}{K} - 1, \tag{1}$$

with $m = 0, \ldots, M-1$. Here, m denotes the frame index within the sensing duration. On the other hand, when the kth band is occupied, the corresponding received samples at the CR are modeled as

$$\bar{Y}_m(\ell) = \bar{X}_m(\ell) + \bar{Z}_m(\ell), \quad \ell = \frac{kN}{K}, \frac{kN}{K} + 1, \ldots, \frac{(k+1)N}{K} - 1, \tag{2}$$

with $m = 0, \ldots, M-1$, where $\bar{X}_m(\ell)$ represents the received PU signal in the ℓth FFT bin and the Mth frame, including the effect of path loss, shadowing and multipath fading. Let $\mathrm{SNR}(p)$, $p = 0, \ldots, L-1$ denote the distinct SNR values of the L PUs, which are assumed to be known. The approach easily extends to the unknown SNR case also, by considering a conservative design that assumes a certain minimum SNR on the occupied bins. This minimum SNR is typically mandated by the primary network, in the form of the minimum SNR at which the CR users are required to be able to sense the primary signal at a certain pre-specified reliability level. The goal of the SS module in the CR is to determine the presence (denoted $\mathcal{H}_1$) or absence (denoted $\mathcal{H}_0$) of the primary signal using the observations $\bar{Y}_m(k)$ described above.

Let $P(k)$ be the average energy over M consecutive frames in the kth band, and P_{tot} be the average energy over all K bands and M frames. Therefore, for $k = 0, 1, \ldots, K-1$ [28,29],

$$P(k) \triangleq \frac{1}{M}\sum_{m=0}^{M-1}\sum_{q=0}^{\frac{N}{K}-1}\left|Y_m\left(\frac{kN}{K}+q\right)\right|^2, \qquad P_{\text{tot}} = \sum_{k=0}^{K-1}P(k).$$

Note that, the above model assumes that the CR is aware of the hop instant of the PU network, i.e., it is aware of the time instants when the PUs possibly change their frequency bands. The hop instants can be determined using the FAR algorithm itself during an initial sensing/calibration phase, where the CR node detects changes in the hop pattern over time. This technique, described in detail in Section 4.1, is used in the hardware implementation of FAR in this paper.

2.2. The FAR algorithm

In this subsection, we briefly describe the detection technique investigated in this paper, namely, the FAR algorithm. This algorithm is same as the FFT-based CFAR detector proposed in [16], which, in turn, is based on the well-known Cell Averaging Constant False Alarm Rate (CA-CFAR) detection technique used in RADAR literature [18]. However, the setup in [16] assumes $L = 1$, as opposed to our case where $L \geq 1$. We work with the FAR algorithm because it is computationally simple, and, therefore, easily implementable on a hardware platform with limited resources. The FAR decision statistic for the kth band is given by [28,29,16]

$$T_M(k) \triangleq \frac{P(k)}{P_{\text{tot}}}, \quad k = 0, \ldots, K-1. \tag{3}$$

The presence of a PU on the kth band is detected by comparing $T_M(k)$ with a threshold τ, as follows:

$$T_M(k) \underset{\mathcal{H}_0}{\overset{\mathcal{H}_1}{\gtrless}} \tau. \tag{4}$$

In the following section, we derive the per-band probabilities of false-alarm (P_{FA}) and signal detection (P_D) of the FAR algorithm, as a function of τ and M, for a given N.

3. Performance analysis and optimization

3.1. Probabilities of false alarm and detection

The following lemma presents the expressions for the false alarm and detection probabilities of the FAR algorithm, denoted by P_{FA} and P_D, respectively.

Lemma 1. *For the FAR algorithm-based detection scheme in (4), the signal detection and false-alarm probabilities are given by:*

$$P_D(k,\gamma,M,N,K,\text{SNR}_{\text{tot}}) = 1 - \frac{\left(\frac{E_{1k}}{G_{1k}}\gamma\right)^{D_{1k}/2}}{\frac{D_{1k}}{2}\mathcal{B}\left(\frac{D_{1k}}{2},\frac{F_{1k}}{2}\right)} \times {}_2\mathcal{F}_1\left(\frac{D_{1k}}{2}, \frac{D_{1k}+F_{1k}}{2}; 1+\frac{D_{1k}}{2}, -\frac{E_{1k}}{G_{1k}}\gamma\right), \tag{5}$$

$$P_{FA}(\gamma,M,N,K,\text{SNR}_{\text{tot}}) = 1 - \frac{(G_0\gamma)^{\frac{MN}{K}}}{\frac{MN}{K}\mathcal{B}\left(\frac{MN}{K},\frac{D_0}{2}\right)} \times {}_2\mathcal{F}_1\left(\frac{MN}{K}, \frac{MN}{K}+\frac{D_0}{2}; 1+\frac{MN}{K}, -G_0\gamma\right), \tag{6}$$

where the parameters are as defined below,

$$G_0 \triangleq 2 - \frac{K-1}{K-1+\frac{1}{N}\text{SNR}_{\text{tot}}}, \qquad D_0 \triangleq \frac{M}{K}\text{SNR}_{\text{tot}} + MN\left\{\frac{3}{2} - \frac{3}{2K} + \frac{K-2+1/K}{2K-2+\frac{4}{N}\text{SNR}_{\text{tot}}}\right\},$$

$$G_{1k} \triangleq 2 - \frac{1}{1+\frac{1}{N}\text{SNR}(k)}, \qquad D_{1k} \triangleq \frac{MN}{K}\left\{\frac{3}{2} + \frac{1}{N}\text{SNR}(k) + \frac{1}{2+\frac{1}{N}\text{SNR}(k)}\right\},$$

$$E_{1k} \triangleq 2 - \frac{K-1}{K-1+\frac{1}{N}\text{SNR}_{\text{tot}}^{(k)}}, \qquad F_{1k} \triangleq \frac{M}{K}\text{SNR}_{\text{tot}}^{(k)} + MN\left\{\frac{3}{2} - \frac{3}{2K} + \frac{K-2+1/K}{2K-2+\frac{4}{N}\text{SNR}_{\text{tot}}^{(k)}}\right\},$$

$$\text{SNR}_{\text{tot}} \triangleq \sum_{p=0}^{L-1}\text{SNR}(p), \qquad \text{SNR}_{\text{tot}}^{(k)} \triangleq \sum_{p=0,\neq k}^{L-1}\text{SNR}(p), \quad \textit{and} \quad \text{SNR}(p) \triangleq \frac{\frac{1}{M}\sum_{m=0}^{M-1}|X_m(p)|^2}{\frac{\sigma^2}{K}} \tag{7}$$

with $\gamma \triangleq \frac{\tau}{1-\tau} \in [0, \infty)$, $\mathcal{B}(\cdot,\cdot)$ *denoting the beta function* [30, *Sec. 8.38*], *and* ${}_2\mathcal{F}_1(\cdot,\cdot;\cdot;\cdot)$ *representing the Gauss' hypergeometric function* [30, *Sec. 9.1*].

Proof. See Appendix A.1. □

With the expressions for the false alarm and detection probabilities in hand, the per-band detection threshold to satisfy a target P_{FA} (or P_D) constraint can be fixed by using numerical techniques. Note that, ${}_2\mathcal{F}_1(a, b; c; d)$ converges if the real part of $c - a + b$ is > 0. Hence, K, N and M should satisfy $\{1 - \frac{2MN}{K} - \frac{D_0}{2}\} > 0$. Substituting for D_0, it is easy to verify that the function converges for all M and N, provided $K > 1$ and $L \geq 1$. Note that $L = 0$ corresponds to the trivial situation when no active PUs are present. The CR can freely transmit in any of the bands in this case.

From the expressions of P_{FA} and P_D, it should be noted that the FAR algorithm is not robust to noise variance uncertainty, as opposed to the CA-CFAR based techniques studied earlier [29,16], the main reason being the presence of multiple PUs. The values of P_{FA} and P_D at a given bin k is not only dependent on SNR(k), but also on SNR_{tot}.

3.2. Optimum sensing duration

Clearly, a longer sensing duration results in more accurate sensing, but leaves less time within each hop duration for data transmission; we wish to find the right trade-off between the two effects. To this end, we now derive the sensing duration that maximizes the CR throughput, subject to a constraint on PU protection. When there are L active PUs, at any time, $K - L$ bands are available, and L bands are busy. On average, the CR correctly declares $(K - L)(1 - P_{FA}(\gamma, M, N, K, \text{SNR}_{\text{tot}}))$ bands as available, and it incorrectly declares $\sum_{k:\mathbf{u}(k)=1}(1 - P_D(k, \gamma, M, N, K, \text{SNR}_{\text{tot}}))$ bands as available. Let $0 \leq \alpha(k) < 1, k = 0, \ldots, K-1$, represents the fractional data rate obtained by the CR when it transmits on the bands occupied by the PUs, after incorrectly declaring them to be free. The value $\alpha(k) = 0, \forall k$ denotes the case where the CR node obtains no usable throughput when it transmits in bands that are actually occupied by PUs. In practice, the data rate achieved on bands occupied by PUs would depend on the relative locations of the PU transmitter, CR transmitter, CR receiver, and the CR and PU transmit powers. Assuming zero rate on such bands is a conservative approach, and serves as an additional protection to the PUs, along with the interference constraint, which will be elaborated on below.

In this paper, we consider the product of the time available for data transmission and the average bandwidth harvested by the CR, denoted by Π, as the performance metric:

$$\begin{aligned}\Pi &\triangleq \mathbb{E}\{K^{(r)} + \alpha K^{(w)}\} W \times (N_h - N_s) \\ &= \Big[(K-L)(1 - P_{FA}(\gamma, M, N, K, \text{SNR}_{\text{tot}})) + \sum_{k:\mathbf{u}(k)=1} \alpha(k)\ (1 - P_D(k, \gamma, M, N, K, \text{SNR}_{\text{tot}}))\Big] W (N_h - N_s). \end{aligned} \tag{8}$$

Analytically optimizing the sensing duration and detection threshold to maximize the above cost function for a general $\alpha(k)$, although possible, would result in messy expressions. Therefore, for simplicity of exposition, we consider the special case of $\alpha(k) = 0, \forall k$. Then, the objective function reduces to

$$\Pi = (K - L)(1 - P_{FA}(\gamma, M, N, K, \text{SNR}_{\text{tot}}))W(N_h - N_s). \tag{9}$$

Observe that, in the above, as N_s increases, $1 - P_{FA}(\gamma, M, N, K, \text{SNR}_{\text{tot}})$ increases, while $N_h - N_s$ decreases; and hence there exists an optimal sensing duration that maximizes Π.

Thus, we state the optimization problem as follows:

$$\max_{N_s, \gamma}\{\Pi\} \text{ subject to } \min_{k:\mathbf{u}(k)=1} P_D(k, \gamma, M, N, K, \text{SNR}_{\text{tot}}) \geq P_{\min} \tag{10}$$

where $P_{\min}$ is the minimum detection probability performance that the CR detector is required to satisfy. Since $N_s = NM$, finding the optimum N_s reduces to finding the optimum M, for a given FFT size N. The value of N can be considered to be fixed, as it is generally taken to be the largest value supported by the SS hardware. Now, for a given γ, it can be shown that Π is concave in $0 \leq M \leq \frac{N_h}{N}$. Also, for a given M, both $P_D(k, \gamma, M, N, K, \text{SNR}_{\text{tot}})$ and $P_{FA}(\gamma, M, N, K, \text{SNR}_{\text{tot}})$ decrease with γ. Hence, Π is maximized when γ is such that the constraint in (10) is satisfied with equality. The following lemma gives the equation which needs to be numerically solved to find the optimum M.

Lemma 2. *Let* $\gamma_{\min}$ *denote the value of* γ *that satisfies* $\min_{k:\mathbf{u}(k)=1} P_D(k, \gamma, M, N, K, \text{SNR}_{\text{tot}}) \geq P_{\min}$ *with equality. Then, the value of* M *which maximizes the cost function in* (9) *is the solution to the equation,*

$$\begin{aligned}&\frac{G_0\gamma_{\min}}{{}_2\mathcal{F}_1(1, 1-BM; 1+AM; -G_0\gamma_{\min})} \times \left\{ \frac{B}{1+AM} {}_2\Theta^{(1)}\left(\begin{matrix} 1, & 1 \\ & 2-BM \end{matrix} \middle| \begin{matrix} 1-BM, & 2-BM, & 2 \\ & 2, & 2+AM \end{matrix} ; G_0\gamma_{\min}, \ G_0\gamma_{\min} \right) \right. \\ &\left. + \frac{A(1-BM)}{(1+AM)^2} {}_2\Theta^{(1)}\left(\begin{matrix} 1, & 1 \\ & 2+AM \end{matrix} \middle| \begin{matrix} 1+AM, & 2, & 2-BM \\ & 2, & 2+AM \end{matrix} ; G_0\gamma_{\min}, \ G_0\gamma_{\min} \right) \right\} \\ &+ (A+B)\log(1 + G_0\gamma_{\min}) - A\log(G_0\gamma_{\min}) + (A+B)\psi^{(0)}(AM + BM)\end{aligned}$$

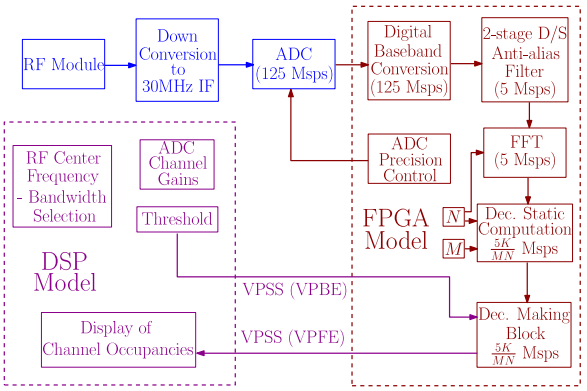

Fig. 2. Block diagram for the implementation on Lyrtech SFF SDR DP.

$$-A\psi^{(0)}(AM) - B\psi^{(0)}(BM) - \frac{N_h}{M(N_h - NM)} = 0, \tag{11}$$

$$\text{with } A \triangleq \frac{N}{K}, \qquad B \triangleq \frac{\left[\left(N - \frac{N}{K}\right) + \frac{1}{K}\text{SNR}_{\text{tot}}\right]^2}{\left(N - \frac{N}{K}\right) + \frac{2}{K}\text{SNR}_{\text{tot}}}, \tag{12}$$

and where $\psi^{(0)}$ is the digamma function, and ${}_2\Theta^{(1)}(\cdot)$ is a Kampé de Fériet-like function [31]*, defined below.*

$${}_2\Theta^{(1)}\left(\begin{matrix} a_1, & a_2 b_1, & b_2, & b_3 \\ & c_1 | d_1, & d_2 & \end{matrix}\middle| x_1, \; x_2\right) \triangleq \sum_{m=0}^{\infty} \frac{(a_1)_m (b_1)_m (b_2)_m (b_3)_m}{(c_1)_m (d_1)_m (d_2)_m} \frac{x_1^m}{m!} \times {}_3\mathcal{F}_2(a_2, b_2 + m, b_3 + m; d_1 + m, d_2 + m; x_2) \tag{13}$$

Also, ${}_3\mathcal{F}_2(\cdot, \cdot, \cdot; \cdot, \cdot; \cdot)$ is a hypergeometric function, and $(a)_m \triangleq \frac{\Gamma(a+m)}{\Gamma(a)}$ is the Pochhammer symbol.

Proof. See Appendix A.2.

Note that the infinite series of the function ${}_2\Theta^{(1)}(\cdot)$ as given by (13) converges very fast. In our simulations, the result obtained from a truncated series with 30 terms was found to be accurate to four decimal places.

4. FAR algorithm on Lyrtech SFF SDR DP

We now describe our implementation of the FAR algorithm on the Lyrtech SFF SDR DP (from here on, called DP for short). The block diagram of the DP is as shown in Fig. 2, and the hardware circuitry is shown in Fig. 3. The DP consists of the following three modules:

1. A *Digital Processing Module* (DPM), with Xilinx Virtex-4 *SX*35 FPGA, TMS320 DM6446 system-on-chip DSP, MSP430 MCU for power management.
2. A *Data Conversion Module* (DCM), with a 14-bit, 125 Msps input channel (ADC), and dual, 16-bit, 500 Msps output channels (DAC). For synchronization, a 10 MHz onboard reference clock is provided, along with two external clock inputs for ADC and DAC.
3. An *RF module* (RFM) with a half-duplex (stackable for full-duplex) receiver operating at RF frequency range of 360–960 MHz, selectable bandwidth of 5/20 MHz, intermediate frequency (IF) at 30 MHz, with an RF input and output gains of up to 22 dB.

Several software development tools are supported by the DP. In particular, we implemented the FAR algorithm on the DPM, using a Model Based Design Kit (MBDK) released by Lyrtech. Since the MBDK works in association with MATLAB® Simulink™, the implementation of all the modules are done in MATLAB Simulink.

The parameters chosen for the implementation are as follows. We chose $B = 5$ MHz with $K = 8$ bands, denoted (in the increasing order of their center frequencies) by $C_4, C_5, C_6, C_7, C_0, C_1, C_2, C_3$. The center frequencies of these bands are 395.6, 396.1, 396.65, 397.23, 393.5, 394.15, 394.8, 395.1 MHz, respectively, representing a total bandwidth of 3.73 MHz. We set $N = 64, M = 128, 256$; larger values were not feasible due to the limitations of the in-built DSP multipliers, in the DPM. We use the NI PXIe1062Q instrument to generate sinusoids, that model the primary user signals. Note that we use the sinusoids as the primary signal, as they are easy to implement as an FH signal on the hardware platform. Similar results would hold for a general band-limited signal also.

Fig. 3. Lyrtech SFF SDR DP circuit board.

The received signal is filtered to a passband of 5 MHz at with center frequency 395.4 MHz, and is down-converted to an Intermediate Frequency (IF) of 30 MHz. The IF signal is sampled at a rate of 125 Msps. The sampled IF signal is digitally down-converted to baseband. The signal is then down-sampled by a factor 25 (since the Nyquist rate required is 5 Msps), each for the in-phase and quadrature components, and is passed to the FFT block, which outputs the corresponding frequency domain signal in groups of N samples. These values are sent to the decision statistic block, where the power in the each band is computed by grouping $\frac{N}{K}$ bins for each band and averaging them over M frames. This calculation corresponds to the FAR statistic, i.e., calculating $T_M(k)$, $k = 1, \ldots, K$, following (4). Then, the detection is carried out by comparing the power in each bin with a user-defined threshold. The decisions made on each band can be made to be seen on a display (800×600) provided in the DPM (Video Processing Back End (VPBE) and Video Processing Front End (VPFE)).

4.1. Primary hop-instant identification

It is important for the CR user to know, and synchronize its operation to the hopping instants of the frequency-hopping primary user. A method for estimating the FH boundary for Bluetooth signal, with help of a Short Time Fourier Transform (STFT), has been discussed in [27]. Based on this approach, we propose a technique to identify the FH boundary by using the already implemented FAR algorithm. This method works under the assumption that all the primary users are hopping synchronously.

The time instant at which the CR user powers up and starts sensing the spectrum will be the reference point in time (from here on, called as the "reference") for all the secondary operations. The operational time of the secondary user is also divided into successive durations of N_h samples starting from the reference, each of which is termed as *Virtual Hopping Period* (VHP) of the secondary user. The CR needs to estimate the difference in time between start of VHP and the start of the hopping period of the primary, within that particular VHP. Let this time lag be defined as N_{offset} samples. The idea is to identify the location in each VHP, where a change in the occupancies of the primary channels occurs. To this end, in each VHP, the spectrum has to be sensed repeatedly to know the occupancies. Let N_{acc} be the difference between the start of successive sensing operations by the CR (ideally, N_{acc} should be equal to 1, but due to hardware and processing limitations, one may have to use a larger N_{acc}). Since the sensing duration of the FAR algorithm is N_s, the samples in the successive sensing operations will be overlapped when $N_s > N_{\text{acc}}$.

The procedure to estimate N_{offset} is as follows. Let an occupancy vector $\bar{U}$ of length K represent the presence or absence of the primary user on each channel, as declared by the CR, with an initial value set to the all zero vector $[0, \ldots, 0]$ for all the K bands. Suppose, N_{est} VHPs are used for estimating the hopping boundary. Starting from the reference, the spectrum is sensed repeatedly after each N_{acc} samples. The threshold for the FAR algorithm is set to satisfy a given, low value of P_{FA}. A vector $\bar{H}$ of length $\frac{N_h}{N_{\text{acc}}}$ is defined with all elements as zeros. Let i_d, $0 \leq i_d \leq \frac{N_h}{N_{\text{acc}}} - 1$ denote the index of the sensing operations performed in one VHP. The occupancy vector $(\bar{U})$ for $(i_d + 1)$th sensing operation is logically XOR-ed with that of the (i_d)th operation. If any one or more entries of the resultant vector is one, then $\bar{H}(i_d + 1)$ is incremented by one. This process is repeated for all values of i_d for N_{est} VHPs. Later, each value of $\bar{H}$ is compared with a threshold h_{thr} and the estimated offset is given by

$$\hat{N}_{\text{offset}} = \{N_{\text{acc}} \times i_d : \; H(i_d) \geq h_{\text{thr}}\}. \tag{14}$$

The value of h_{thr} is chosen through simulations.

As an example, consider a case where $N_{\text{offset}} = 1040$. It is assumed that $N_h = 2^{12}$, $N_{\text{est}} = 100$, and the SNR = 6 dB, for each active user. Since $N_{\text{acc}} = NM$, and the choice of N is constrained by the hardware, $N = 16$ is chosen as the FFT size. Therefore, the choosing N_{acc} depends on the choice of M. Note that as M increases, the detection accuracy increases, but the resolution of the boundary detection decreases. For this example, we will consider $M = 1$, and $M = 32$. A threshold value

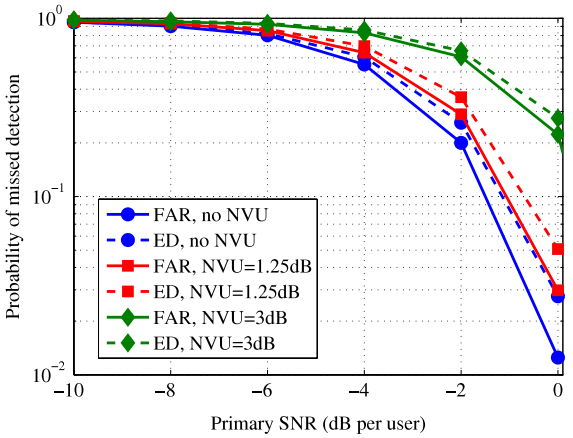

Fig. 4. Comparison of FAR with the conventional ED [6], with and without Noise Variance Uncertainty (NVU). Here, $N = 64$, $M = 128$, $L = 3$, and the detectors are designed with a target false alarm probability of 0.01.

of 0.3 is chosen for FAR algorithm. The histogram $\bar{H}$ is computed, and the value of the threshold h_{thr} is set to be 85 (chosen through simulations). With these values, for the case of $M = 1$, it is seen that the above mentioned boundary identification procedure gave the boundary change index as 65, which results in $65 \times 16 \times M = 1040 = N_{\text{offset}}$. Similar exercise with $M = 32$ gave the boundary change index as 2, which implies $2 \times 16 \times M = 1040 = N_{\text{offset}}$.

Thus, a secondary user can identify the hopping boundary of the FH primary signal where all the primary users are hopping synchronously. This method can be applied with slight modifications to the case where the primary users when they are not hopping synchronously, by suitably choosing the threshold for the histogram. More details can be found in [27].

5. Results

5.1. Monte Carlo simulations

Our simulation setup is chosen to match the hardware setup explained in the previous section, with $N = 64$, $M = 16$, $K = 8$ and $L = 2$ PUs. We consider the performance of the detector for each of the different bands. For ease of presentation, suppose that the two PUs are active in bands C_0 and C_7, at a given point in time. For evaluating the algorithms, it is sufficient to condition on this particular occupying pattern, by the symmetry of the problem. That is, we get the same CR performance conditioning on any pair of occupied bins.

In Fig. 4, we compare the detection performance of the FAR algorithm with ED [6], with and without uncertainty in the noise variance. The noise uncertainty model assumed is the same as in past work [7], namely, that the noise variance is unknown, but lies in a range of $[\sigma_n^2 - x \text{ dB}, \sigma_n^2 + x \text{ dB}]$, where x is the noise variance uncertainty, and σ_n^2 is the nominal noise variance. Then, the detector is designed to meet a false alarm probability target of 0.01 at a noise variance of $\sigma_n^2 + x$ dB, and the probability of detection performance is evaluated at a noise variance of $\sigma_n^2 - x$ dB. The plot shows that the FAR algorithm outperforms ED, and offers about 0.5–1 dB improvement in the primary SNR required to achieve a given probability of detection. Thus, the FAR is a better decision statistic compared to the energy in the band, for detection of FH primary signals, in the presence of noise uncertainty. In Fig. 5, we plot the effective CR throughput as a function of the sensing duration, with $N_h = 1024$. For larger primary SNR, the highest CR throughput is obtained at a shorter sensing duration, as expected. This is because, when N_s is fixed, the detection performance increases with SNR. Given the protection requirement from the primary, the CR can decrease N_s, while ensuring adequate protection. This makes $N_h - N_s$ larger and increases the throughput. Also, in terms of the effective throughput, the FAR and ED perform almost equally well. This is because the throughput is a relatively insensitive function of the detector performance, and, hence, detectors with similar performance would yield average throughputs that are only marginally different from each other.

In Fig. 6, we plot the simulated optimal throughput (i.e., simulated value of the cost function in (9)) and its corresponding theoretical throughput calculated using the expressions in (5) and (6), for various SNR values. It is seen that in the low SNR regime, the accuracy of theoretical calculations become looser. As SNR increases, the approximation becomes tighter. This happens because of the approximation used in Lemma 1 [32].

Fig. 7 shows the variation of the optimal value of M as a function of the interference limit P_{min}. The hopping duration N_h is set to 1024, $L = 2$ primary users, and the SNR values are fixed to be $[-5, -5]$ dB at $[C_0, C_7]$, respectively. The theoretical curves are obtained by numerically solving (11) to obtain a real-valued M. We then evaluate the throughput for the two nearby integer values of M, and pick the optimal M as the value that offers the better throughput. For obtaining the simulated curves, we sweep over a range of detection thresholds and different values of M, and pick the combination that offers the best CR throughput. The good match between theoretical and simulated curves validates the optimization of the

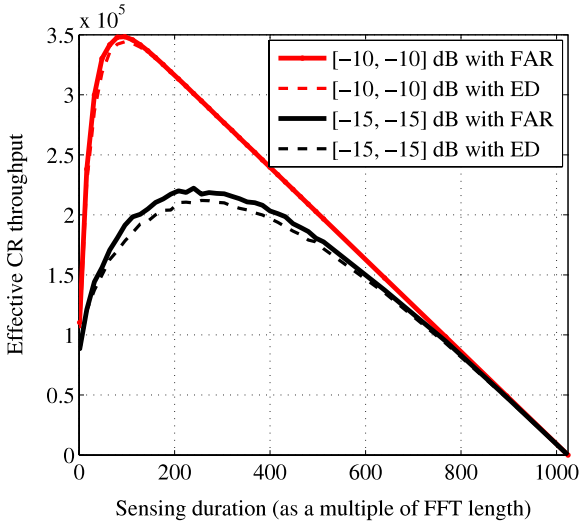

Fig. 5. Comparison of CR throughput obtained by FAR algorithm with that of ED, obtained through hardware implementation, with $N = 64$. The two numbers in the legends, for e.g., $[-10, -10]$ dB, indicate the SNRs of the two PUs present in bands C_0 and C_7.

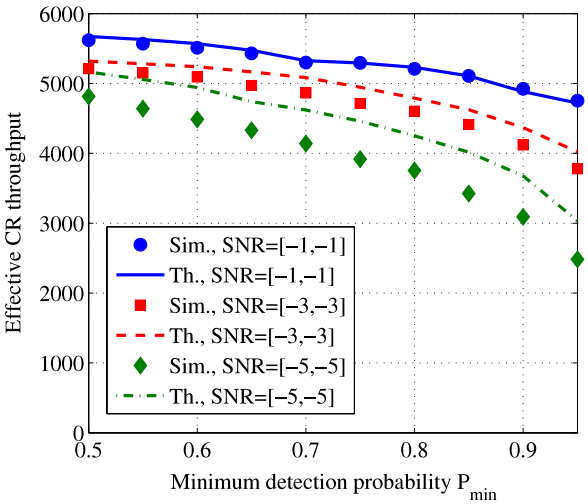

Fig. 6. Optimal throughput for $N = 64$, $N_h = 1024$. For the simulation result, the optimal throughput was obtained by sweeping a range of M and threshold, and choosing the pair that offered the best throughput.

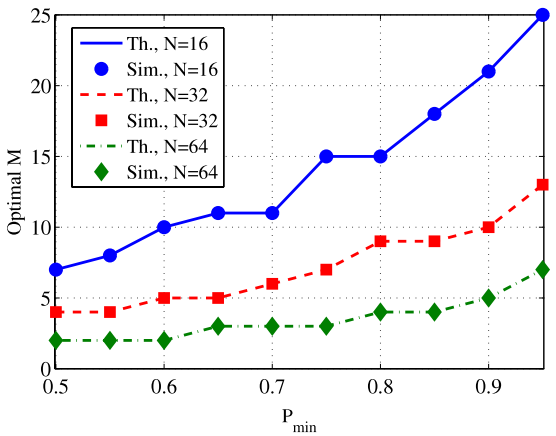

Fig. 7. Comparison of optimal number of frames M for different values of the FFT size N, for $L = 2$, and $N_h = 1024$ samples. Notice that as N varies, the optimal M varies such that NM is roughly the same, for each given P_{min}.

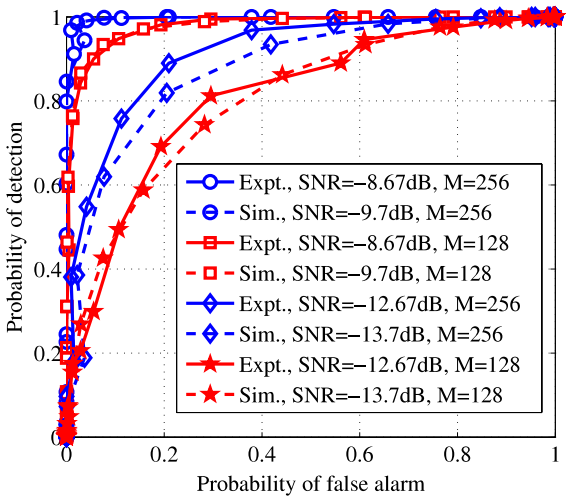

Fig. 8. Comparison of ROCs from simulations and experiments, at different M and SNRs. The implementation loss is about 1 dB. The legends, Sim. and Expt., indicate the curves obtained due to Monte Carlo simulations and hardware experiments, respectively.

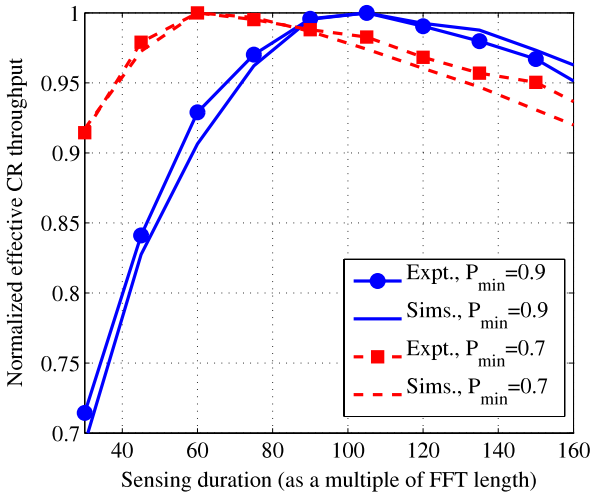

Fig. 9. Optimum CR throughput Vs. N_s, comparing the hardware implementation with simulated curves, for $N = 64$.

CR throughput presented in Section 3.2. Also, we notice that as N varies, for each given $P_{\min}$, the optimal M is such that NM is roughly constant. For example, at $P_{\min} = 0.9$, the optimal M is 5, 10 and 21 for $N = 16$, 32 and 64, respectively. This is because the detection performance, and, consequently, the effective throughput, is primarily determined by the sensing duration, which equals NM.

5.2. Experimental results from the Lyrtech SFF SDR DP

For the experimental results, we generated a pure sinusoidal FH primary signal using the National Instruments PXI signal generator, and evaluated the performance at the band corresponding to C_0, with a center frequency of 393.5 MHz. The SNR at the CR sensor was set by first calibrating the noise floor in the absence of the primary signal, and then setting the transmit power of the primary so that the received signal power meets the required target.

In Fig. 8, we plot the Receiver Operating Characteristic (ROC) curves for different values of M and primary SNR. As expected, the detection performance improves with M and SNR. We observe that the experimental curves follow the same trends as the theoretical curves, allowing for an implementation loss of about 1 dB in the primary SNR. We attribute the difference to the effect of quantization in the fixed-point implementation (and perhaps other hardware non-idealities, e.g., in the RF front-end filters) used in the hardware platform.

Finally, in Fig. 9, we show the normalized optimal throughput of the CR, normalized to its maximum attainable value at the given $P_{\min}$, as a function of the sensing duration N_s, comparing the throughput observed from the DP with that observed via simulations. The experimental results were generated by using a CR transmitter that sends data at a rate of 20.833 Msps,

a primary transmit power of −107.5 dBm, a hopping duration of $N_h = 6.5$ ms, and about 5 m distance between the primary transmitter and CR spectrum sensing node. The simulation results were generated using the setup described in the previous subsection, at a primary SNR of −10 dB at the CR node. The good match between the two sets of plots is clear from the graph, validating our implementation. Also, the optimal sensing duration is larger for larger minimum detection probability performance $P_{\min}$.

6. Conclusions

In this paper, we considered the problem of spectrum sensing in the presence of a multiuser frequency-hopping primary network. We theoretically analyzed the performance of the FAR algorithm, and validated the results through simulations. The sensing duration that maximizes the throughput of the CR system, under a constraint on the interference to the primary network was derived. A technique to synchronize the CR system with the primary hopping instants was presented. The FAR algorithm was implemented on Lyrtech SFF SDR DP and its performance was benchmarked by the ROCs obtained from Monte Carlo simulations. An implementation loss of about 1 dB was observed in the hardware implementation.

Appendix A

A.1. Proof of Lemma 1

Under $\mathcal{H}_0$, $\bar{Y}_m = Q\bar{y}_m = Q\bar{z}_m$ is i.i.d. Gaussian with mean 0 and covariance $\sigma^2\mathbf{I}_N$, since Q is a unitary transform. Similarly, under $\mathcal{H}_1$, $\bar{Y}_m$ is jointly Gaussian with mean $\bar{X}_m = Q\bar{x}_m$ and covariance $\sigma^2\mathbf{I}_N$. Now, the statistic

$$T_M(k) = \frac{P(k)}{P_{\text{tot}}} = \frac{P(k)}{P(k) + \sum_{y=0,\neq k}^{K-1} P(y)} = \frac{1}{1 + \frac{\sum_{y=0,\neq k}^{K-1} P(y)}{P(k)}}; \quad \text{and therefore,}$$

$$T_M(k) \underset{\mathcal{H}_0}{\overset{\mathcal{H}_1}{\gtrless}} \tau, \qquad \Rightarrow \frac{P(k)}{P_{\text{tot}} - P(k)} \underset{\mathcal{H}_0}{\overset{\mathcal{H}_1}{\gtrless}} \frac{\tau}{1-\tau}. \tag{15}$$

Following the above result, Let

$$T_k \triangleq \sum_{m=0}^{M-1} \sum_{q=0}^{\frac{N}{K}-1} \left| \frac{Y_m\left(\frac{N}{K} \times k + q\right)}{\sigma/\sqrt{2}} \right|^2, \qquad S_k \triangleq \sum_{\ell=0,\ell\neq k}^{K-1} T_\ell. \tag{16}$$

Then, if $F^{\mathcal{H}_0}_{T_M(k)}(\tau)$ represents the CDF of $T_M(k)$ under $\mathcal{H}_0$,

$$F^{\mathcal{H}_0}_{T_M(k)}(\tau) = \Pr\left\{ \frac{T_k}{S} \leq \frac{\tau}{1-\tau} \mid \mathcal{H}_0 \right\}. \tag{17}$$

Now, let $\mathcal{K}\mathcal{X}^2_{\Theta}(\Psi)$ represent a chi-squared random variable (RV) with Θ Degrees of Freedom (DoF), non-centrality parameter Ψ and a scaling factor $\mathcal{K}$. It is easy to see that under $\mathcal{H}_0$, $T_k \sim \mathcal{X}^2_{\frac{2MN}{K}}(0)$, $k = 1, 2, \ldots, K-1$. Also, $S_k \sim \mathcal{X}^2_{2M\left(N-\frac{N}{K}\right)}\left(\frac{2M}{K}\sum_{p=0}^{L-1} \text{SNR}(p)\right)$. Next, we use a result due to Patnaik [32,6], which approximates a $\mathcal{X}^2_{\Theta}(\Psi)$ RV with a $G\mathcal{X}^2_{\Omega}(0)$ RV, where $\Omega \triangleq \frac{(\Theta+\psi)^2}{\Theta+2\psi}$ and $G \triangleq \frac{\Theta+\psi}{\Theta+2\psi}$. Using this and the notations in (7), it follows that $S_k|\mathcal{H}_0 \sim G_0\mathcal{X}^2_{D_0}(0)$ and $T_k|\mathcal{H}_0 \sim \mathcal{X}^2_{\frac{2MN}{K}}(0)$.

Let $\gamma \triangleq \frac{\tau}{1-\tau}$. Since the statistic $T_M(k)$ is a ratio of scaled chi-squared RVs, it follows a four-parameter beta prime distribution, i.e., [33, chap. 25],

$$T_M(k) = \frac{T_k}{S_k} \sim \beta'\left(\frac{MN}{K}, \frac{D_0}{2}, 1, \frac{1}{G_0}\right), \quad \text{with PDF}$$

$$f^{\mathcal{H}_0}_{T_M(k)}(\nu) = \frac{(G_0\,\gamma)^{\frac{MN}{K}}\,(1+G_0\gamma)^{-\frac{MN}{K}-\frac{D_0}{2}}}{\frac{MN}{K}\,\mathcal{B}\left(\frac{MN}{K}, \frac{D_0}{2}\right)} \tag{18}$$

for $\gamma \in [0, \infty)$. The expression for P_{FA} follows from calculating the CDF. A similar analysis for the statistic under $\mathcal{H}_1$ gives the expression of P_D.

In addition to the above derivation, we have also verified the accuracy of the derived expressions through simulations, which we do not present in the paper due to lack of space.

A.2. Proof of Lemma 2

First, note that Π is concave in $0 \leq M \leq \frac{N_h}{N}$. Hence, it suffices to pick the M that satisfies $\frac{\partial \Pi}{\partial M} = 0$. Define A and B, as in (12). Using (6), (9), and a transformation result for the Gauss' hypergeometric function [30, Sec. 9.131], Π can be rewritten as:

$$\Pi = K' \left[\frac{\Gamma(AM + BM)}{AM\,\Gamma(AM)\Gamma(BM)} \times (G_0\gamma_{\min})^{AM} \times (1 + G_0\gamma_{\min})^{1-AM-BM}\, {}_2\mathcal{F}_1\,(1,\, 1 - BM;\, 1 + AM;\, -G_0\gamma_{\min}) \right],$$

where $K' \triangleq (K - L)(N_h - NM)$. Ancarani and Gasaneo [31] have derived the following partial derivatives of the Gauss' hypergeometric function ${}_2\mathcal{F}_1(a, b; c; d)$ with respect to b and c:

$$\frac{\partial\, {}_2\mathcal{F}_1}{\partial b} = \frac{d}{b}\frac{ab}{c}\, {}_2\Theta^{(1)}\left(\begin{matrix} 1, & 1|b, & 1+b, & 1+a \\ & 1+b|2, & 1+c & \end{matrix} \middle|; d, \; d \right), \tag{19}$$

$$\frac{\partial\, {}_2\mathcal{F}_1}{\partial c} = -\frac{d}{c}\frac{ab}{c}\, {}_2\Theta^{(1)}\left(\begin{matrix} 1, & 1|c, & 1+a, & 1+b \\ & 1+c|2, & 1+c & \end{matrix} \middle|; d, \; d \right). \tag{20}$$

The rest of the proof follows by calculating $\frac{\partial \Pi}{\partial M}$, equating it to zero and simplifying further by taking out the common factors. We skip the details as they are straightforward.

References

[1] S. Gurugopinath, R. Akula, C.R. Murthy, R. Prasanna, B. Amrutur, Spectrum sensing with a frequency-hopping primary: from theory to practice, in: Proc. ICC, pp. 1–6.
[2] J. Mitola, G. Maguire, Cognitive radio: Making the software radios more personal, IEEE Pers. Commun. 23 (1999) 201–220.
[3] T. Yucek, H. Arslan, A survey of spectrum sensing algorithms for cognitive radio applications, IEEE Commun. Surveys Tuts. 11 (2009) 116–130.
[4] I.F. Akyildiz, B.F. Lo, R. Balakrishnan, Cooperative spectrum sensing in cognitive radio networks: A survey, Phys. Commun. 4 (2011) 40–62.
[5] K.E. Baddour, Y. Bar-Ness, O.A. Dobre, M. Öner, E. Serpedin, U. Spagnolini, Special issue on cognitive radio: The road for its second decade, Phys. Commun. 9 (2013) 145–147.
[6] H. Urkowitz, Energy detection of unknown deterministic signals, Proc. IEEE 55 (1967) 523–531.
[7] R. Tandra, A. Sahai, SNR walls for signal detection, IEEE J. Sel. Topics Signal Process. 2 (2008) 4–17.
[8] D. Bhargavi, C.R. Murthy, Performance comparison of energy, matched-filter and cyclostationarity-based spectrum sensing, IEEE Eleventh International Workshop on Signal Processing Advances in Wireless Communications (SPAWC) (2010) 1–5.
[9] A. Arriagada, H.-y. Pan, J. Yan, D. Kimball, L. Larson, A wideband high dynamic range frequency hopping transceiver for the joint tactical radio system, in: Proc. MILCOM, pp. 2009–2013.
[10] J.K. Holmes, Spread Spectrum Systems for GNSS and Wireless Communications, Artech House, 2007.
[11] I. Akyildiz, W. Su, Y. Sankarasubramaniam, E. Cayirci, Wireless sensor networks: A survey, Computer Networks 38 (2002) 393–422.
[12] D.-C. Oh, Y.-H. Lee, Low complexity FFT based spectrum sensing in bluetooth system, in: Proc. VTC, pp. 1–5.
[13] G.R. Cooper, Detection of frequency-hop signals, IEEE MILCOM 1 (1986) 1–5.
[14] L. Miller, J. Lee, D. Torrieri, Frequency-hopping signal detection using partial band coverage, IEEE Trans. Aerosp. Electron. Syst. 29 (1993) 540–553.
[15] R.A. Dillard, G.M. Dillard, Likelihood-ratio detection of frequency-hopped signals, IEEE Trans. Aerosp. Electron. Syst. 32 (1996) 543–553.
[16] D. Kun, N.A. Morgan, A new low-cost CFAR detector for spectrum sensing with cognitive radio systems, IEEE Aerosp. Conf. (2008) 1–8.
[17] D. Shnidman, Radar detection probabilities and their calculation, IEEE Trans. Aerosp. Electron. Syst. 31 (1995) 928–950.
[18] J. Lehtomäki, Analysis of Energy Based Signal Detection (Ph.D. thesis), University of Oulu, 2005.
[19] Y. Hur, J. Park, K. Kim, J. Lee, K. Lim, C. H. Lee, S.H. Kim, J. Laskar, A cognitive radio (CR) testbed system employing a wideband multi-resolution spectrum sensing (MRSS) technique, Proc. VTC (2006) 1–5.
[20] Z. Peng, Q. Robert, N. Guo, Demonstration of spectrum sensing with blindly learned features, IEEE Commun. Lett. 15 (2011) 548–550.
[21] M. Hamid, N. Bjorsell, W. Van Moer, K. Barbe, S. Slimane, Blind spectrum sensing for cognitive radios using discriminant analysis: A novel approach, IEEE Trans. Instrum. Meas. 62 (2013) 2912–2921.
[22] H. Zamat, B. Natarajan, Practical architecture of a broadband sensing receiver for use in cognitive radio, Phys. Commun. 2 (2009) 87–102. Cognitive Radio Networks: Algorithms and System Design.
[23] V. Iglesias, J. Grajal, M. Sanchez, M. Lopez-Vallejo, Implementation of a real-time spectrum analyzer on fpga platforms, IEEE Trans. Instrum. Meas. 64 (2015) 338–355.
[24] Z. Khan, J. Lehtomaki, L. DaSilva, M. Latva-aho, Autonomous sensing order selection strategies exploiting channel access information, IEEE Trans. Mobile Comput. 12 (2013) 274–288.
[25] Y.-C. Liang, Y. Zeng, E. Peh, A.T. Hoang, Sensing-throughput tradeoff for cognitive radio networks, IEEE Trans. Wireless Commun. 7 (2008) 1326–1337.
[26] G.H. Raz, A mathematical model and simulation of frequency hopping interferences to FM systems, Math. Comput. Model. 11 (1988) 988–993.
[27] A. Gok, S. Joshi, J. Villasenor, C. Danijela, Estimating the number of frequency hopping interferers using spectral sensing with time and frequency offset measurements, IEEE MILCOM (2009) 1–7.
[28] R.S. Walker, The detection performance of FFT processors for narrowband signals, Technical Report, Defence Research and Development Canada, 1982.
[29] S. Wang, R. Inkol, Theoretical Performance of the FFT Filter Bank-Based Summation Detector, Technical Report, Defence Research and Development Canada, 2005.
[30] I. Gradshteyn, I. Ryzhik, Tables of Integrals, Series and Products, 7th ed, Academic Press, 2007.
[31] L.U. Ancarani, G. Gasaneo, Derivatives of any order of the hypergeometric function ${}_2F_1(a, b; c; z)$ with respect to the parameters a, b and c, J. Phys. A: Math. Theor. 43 (2010) 085210.
[32] P.B. Patnaik, The non-central χ^2- and F-distribution and their applications, Biometrika 36 (1949) 202–232.
[33] N. Johnson, S. Kotz, N. Balakrishnan, Continuous Univariate Distributions, vol. 2, 2 ed, Wiley & Sons, 1995.

Sanjeev Gurugopinath received the B. E. degree in Electrical Engineering from Dr. Ambedkar Institute of Technology, Bangalore in 2004, and the M. Tech. degree in Digital Electronics and Communication Engineering from M. S. Ramaiah Institute of Technology, Bangalore in 2006, both from Visvesvaraya Technological University, Belgaum. Since Jan 2008, he is working towards his Ph.D. at the Signal Processing for Communications Laboratory, at the Electrical Communication Engineering Department, Indian Institute of Science, Bangalore under the supervision of Prof. Chandra R. Murthy.

His research interests are in the areas of detection and estimation theory, information theory and statistics, and cross-layer optimization as applied to spectrum sensing in cognitive radio networks.

Raghavendra Akula was born in Rajahmundry(India) in 1987. He received his B.Tech degree in Electronics and Communication Engineering, from SASTRA University, Thanjavur (India) and M.E. degree in Telecommunication Engineering from Indian Institute of Science, Bangalore (India) in 2009 and 2012 respectively.

Chandra R. Murthy (S'03–M'06–SM'11) received the B.Tech. degree in Electrical Engineering from the Indian Institute of Technology, Madras in 1998, the M.S. and Ph.D. degrees in Electrical and Computer Engineering from Purdue University and the University of California, San Diego, in 2000 and 2006, respectively.

From 2000 to 2002, he worked as an engineer for Qualcomm Inc., where he worked on WCDMA baseband transceiver design and 802.11b baseband receivers. From Aug. 2006 to Aug. 2007, he worked as a staff engineer at Beceem Communications Inc. on advanced receiver architectures for the 802.16e Mobile WiMAX standard. In Sept. 2007, he joined as an assistant professor at the Department of Electrical Communication Engineering at the Indian Institute of Science, where he is currently working.

His research interests are in the areas of Cognitive Radio, Energy Harvesting Wireless Sensors and MIMO systems with channel-state feedback. He is currently serving as an associate editor for the IEEE Signal Processing Letters and as an elected member of the IEEE SPCOM Technical Committee for the years 2014–16.

Prasanna R. was born in Vellore, Tamil Nadu (India) in 1989. He received his B.E degree in Electronics and Communication Engineering, from College of Engineering, Guindy, Chennai(India) and M.E.degree in Microelectronic Systems from Indian Institute of Science, Bangalore (India) in 2010 and 2012 respectively. Since then he has been part of Texas Instruments' R&D Centre in Bangalore.

Bharadwaj Amrutur Bharadwaj Amrutur got a B.Tech in CS&E from IIT Bombay at Mumbai in 1990 and a MS and Ph.D. in EE from Stanford University in 1994 and 1999 respectively. His Ph.D. thesis was on Fast Low Power SRAM Design. From 1999 to 2001, he was employed at Agilent Labs, Palo Alto, CA where he primarily worked on High Speed Chip to Chip interconnects. The highlight of his stay there was the development of a new serial line code called 64B/66B, which has become a part of the 10Gb Ethernet Standard. From 2001 to 2004, he was employed at Greenfield Networks, Sunnyvale, CA, where he worked on two networking ASICs for high speed packet processing applications. Since 2004, he is an Associate Professor at the department of ECE, at the Indian Institute of Science, Bangalore.